Supplementary Information

S1. Characterization of CVD-grown graphene films by Raman spectroscopy

We performed Raman spectroscopy measurements to characterize our large-area CVD-grown graphene films. Figure S1(a) shows three typical Raman spectra obtained from our samples. As shown in Fig. S1(a), two main peaks are clearly observed in all of the spectra at ~1580 cm^{-1} and ~2680 cm^{-1} corresponding to G-band and 2D-band peaks, respectively.[1–3] However, these spectra include distinctive features. First, the full width at half maximum (FWHM) of the 2D-band peaks in the three spectra are ~30 cm^{-1} (blue, spectrum 1), ~40 cm^{-1} (green, spectrum 2), and ~60 cm^{-1} (red, spectrum 3). Second, the intensity ratios between the 2D and G peaks (I_{2D}/I_G) in the three spectra are calculated as 3.8 (blue, spectrum 1), 2.3 (green, spectrum 2), and 0.8 (red, spectrum 3). The FWHM of the 2D-band peak and the I_{2D}/I_G ratio of exfoliated single-layer graphene are 24 cm^{-1} and 3.79, respectively.[1–3] Therefore, spectrum 1 is assigned as the Raman spectrum corresponding to a region of single-layer graphene. In the same manner, spectrum 2 and spectrum 3 are assigned as Raman spectra corresponding to a region of double-layer graphene and a region of triple-layer graphene, respectively.[1–3]

Next, we carried out spatially resolved Raman spectroscopy to estimate the average layer number for our large-area CVD-grown graphene films. Figure S1(b) shows a color map of the FWHM of the 2D-band peak over a 15 μm × 15 μm area. The FWHM values of the 2D-band peak range from 20 cm^{-1} (blue) to 60 cm^{-1} (red). As shown in Fig. S1(a), most of our sample exhibits green-color areas (FWHM of 2D band peak of ~40 cm^{-1}), which corresponds to double-layer graphene; we concluded that the average layer number of our sample is 2.

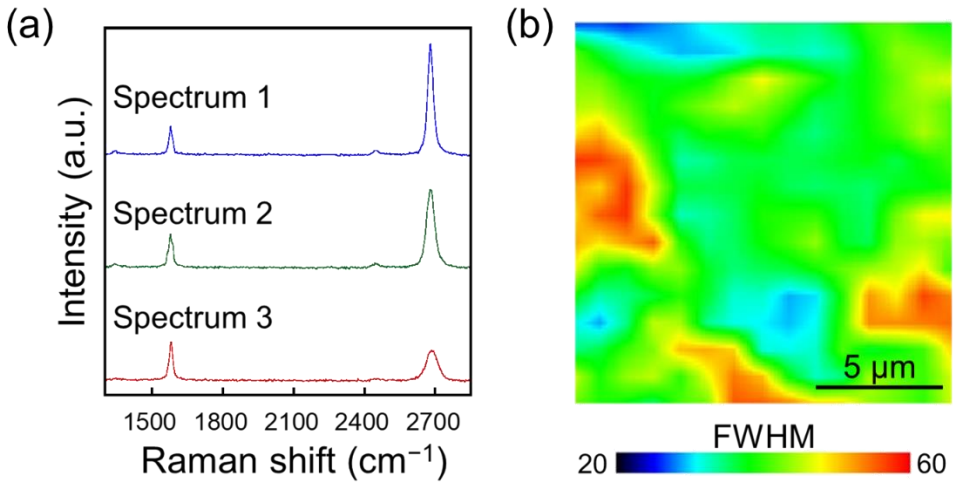

Fig. S1 a Typical Raman spectra of our graphene samples. The FWHMs of the 2D-band peaks in the three spectra are ~30 cm^{-1} (spectrum 1), ~40 cm^{-1} (spectrum 2), and ~60 cm^{-1} (spectrum 3), respectively. The I_{2D}/I_G ratio of the three spectra are calculated as 3.8 (spectrum 1), 2.3 (spectrum 2), and 0.8 (spectrum 3). **b** Two-dimensional color map of the FWHM of the 2D band over a 15 μm × 15 μm area. The scale bar corresponds to 5 μm.

S2. The elapsed time dependence of the sheet resistance ratio with a lower-density ODCB solution

We also investigated the elapsed time dependence of the sheet resistance ratio (R/R_0) using a lower density ODCB solution of $Mes_2B^+[(C_6F_5)_4B]^-$ (0.3 mg/mL) in a N_2-filled glove box. As shown in Fig. S2, the necessary doping times are quite similar for the saturated ODCB solution (30 mg/mL) and the lower-density ODCB solution (0.3 mg/mL). However, we obtain a slight difference in the achieved R/R_0 values between these two ODCB solutions, suggesting the possible work function controllability of our doping method.

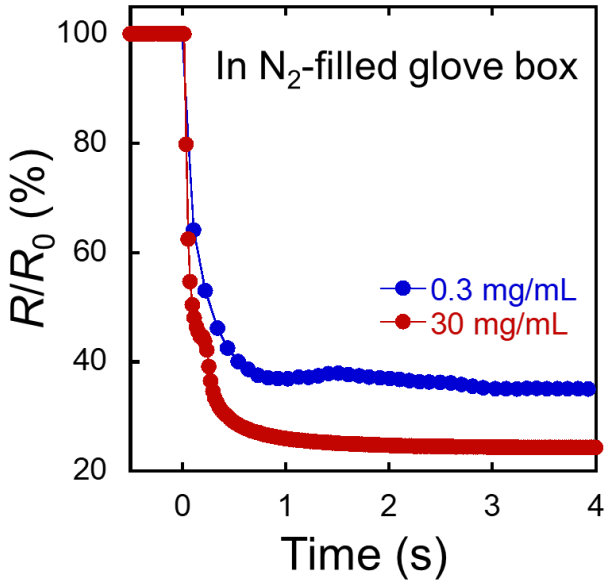

Fig. S2 The comparison of elapsed time dependencies of the sheet resistance ratio for the lower-density (0.3 mg/mL) and saturated (30 mg/mL) ODCB solutions. The time of 0 s corresponds to the time when the ODCB solution of $Mes_2B^+[(C_6F_5)_4B]^-$ was dropped.

S3. Electrical and optical properties of independently prepared graphene samples on a glass substrate after doping with $Mes_2B^+[(C_6F_5)_4B]^-$

Table S1. Electrical and optical properties of independently prepared and rinsed graphene samples on a glass substrate after doping with $Mes_2B^+[(C_6F_5)_4B]^-$.

	Pristine R_0 (Ω/sq)	Doped R (Ω/sq)	$R/R_0 \times 100$ (%)	ΔT at 550 nm (%)	Doped hole density ($\times 10^{14}$ cm^{-2})
Sample #1	837	207	24.7	0.63	2.3
Sample #2	762	229	30.0	0.09	2.6
Sample #3	1161	254	21.8	0.62	3.0
Sample #4	837	204	24.4	0.30	1.1
Sample #5	702	224	32.0	0.63	3.8
Sample #6	1082	197	18.2	–	–
Sample #7	1144	193	16.9	–	–

Average	–	–	24.0±5.61	0.44±0.23	2.57±0.98

Figure S3 shows the comparison of sheet resistance ratio (R/R_0) for the pristine sample, the doped sample before rinsing with dry ODCB, and the doped sample after rinsing in a N_2-filled glove box. It should be noted that the resistance ratios of the doped graphene sample before rinsing and after rinsing are very similar, suggesting the strong interaction between the dopant and graphene film.

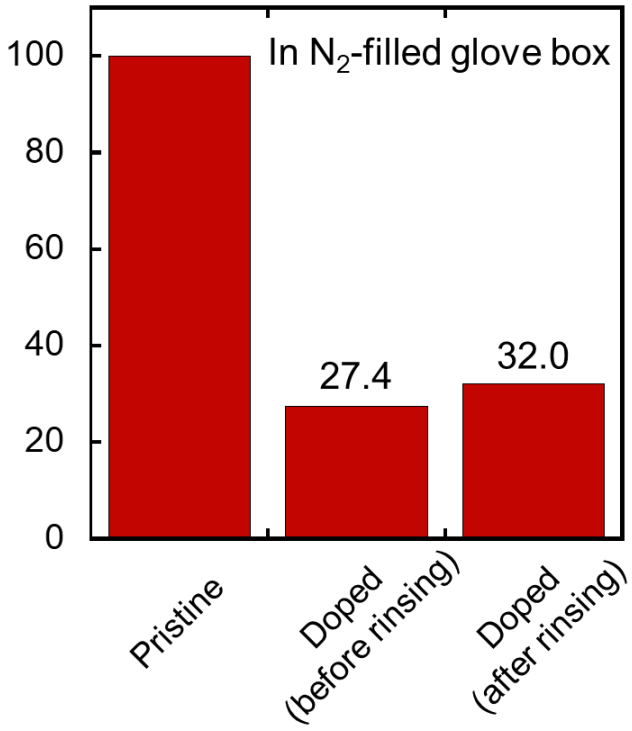

Fig. S3 A comparison of the sheet resistance ratio (R/R_0) for the pristine sample, doped sample before rinsing with dry ODCB, and doped sample after rinsing.

S4. Optical properties of independently prepared unrinsed and rinsed graphene samples on a PET substrate after doping with $Mes_2B^+[(C_6F_5)_4B]^-$

Table S2. Optical properties of independently prepared unrinsed and rinsed graphene samples on a PET substrate after doping with $Mes_2B^+[(C_6F_5)_4B]^-$.

	ΔT at 550 nm (%)
Unrinsed sample #1	2.93
Unrinsed sample #2	13.24
Unrinsed sample #3	14.32
Unrinsed sample #4	2.16
Unrinsed sample #5	0.71
Average	6.65±6.55
Rinsed sample #1	0.20
Rinsed sample #2	0.41
Rinsed sample #3	1.68
Rinsed sample #4	1.88
Average	1.04±0.86

S5. The ΔT values at 550 nm and the sheet resistance ratios (R/R_0) for doped graphene samples prepared by solution-based doping methods

Table S3. A comparison of the ΔT values at 550 nm and the sheet resistance ratios (R/R_0) for doped graphene samples prepared by solution-based doping methods.

Dopant	$R/R_0 \times 100$ (%)	ΔT at 550 nm (%)	Reference number in manuscript
$Mes_2B^+[(C_6F_5)_4B]^-$ (This work)	24.0±5.61	0.44±0.23	–
HNO_3	39.7	0.6	3
$AuCl_3$	33.5	2.0	18
TFSA	30.4	2.2	19
$Mo(tfd\text{-}COCF_3)_3$	68.3	4.7	20

Magic blue	43.9	3.2	20
$Mo(PhBz\text{-}dt)_3$	94.3	3.1	20
$AuCl_3$	30.1	6.7	23
$RhCl_3$	47.9	4.7	23
HNO_3	68.5	1.7	23
$AuCl_3$	23.9	1.3	25
TFSA	31.1	1.1	25

S6. The time-dependent changes in the R/R_0 value

Table S4. A comparison of time-dependent changes in the R/R_0 value for the doped graphene sample with those of previously reported solution-based hole-doping reagents under ambient conditions.

Dopant	Initial $R/R_0 \times 100$ (%)	$R/R_0 \times 100$ (%)	Reference number in manuscript
$Mes_2B^+[(C_6F_5)_4B]^-$ (This work)	24.7	28.6 (31 days after)	–
$AuCl_3$	25.1	27.8 (20 days after)	18
TFSA	32.0	32.9 (30 days after)	19
$AuCl_3$	30.1	35.9 (20 days after)	23
$RhCl_3$	47.9	56.3 (20 days after)	23
HNO_3	68.5	130.86 (20 days after)	23
$AuCl_3$	23.9	35.6 (35 days after)	25
TFSA	42.3	47.6 (32 days after)	25

S7. Fabrication of organic photovoltaic cells with doped graphene electrodes

We used graphene films doped with $Mes_2B^+[(C_6F_5)_4B]^-$ as the anode material in organic photovoltaic cells (OPVs). In these OPVs, we prepared single-layer graphene (SLG) and double-layer graphene (DLG) films by a thermal CVD method using CH_4 gas as the carbon feedstock at ambient pressure. The SLG and DLG films were grown on Cu(111)/sapphire and Cu–Ni alloy (111)/sapphire catalysts, respectively.[4,5] We doped hole carriers into the SLG and DLG using $Mes_2B^+[(C_6F_5)_4B]^-$, as shown in Fig. 2(a) of the main text. Figure S4(a) shows a schematic of the device structure. A MoO_3 layer (15 nm thick) was deposited onto the anode material by vacuum evaporation. As an active layer, we selected a blend of a small-bandgap semiconducting polymer donor (thieno[3,4-b] thiophene/benzodithiophene (PTB7)) and acceptor ([6,6]-phenyl-C_{71}-butyric acid methyl ester ($PC_{71}BM$)). For comparison, we fabricated the OPVs using both pristine and doped graphene films.

Figure S4(b) shows the short-circuit current density (J_{sc})–voltage characteristics of OPVs fabricated by pristine and doped graphene films. The J_{SC}–voltage characteristics were measured using a source meter (Keithley, model 2400) under one-sun AM 1.5G simulated sunlight (100 mW cm^{-2}) with a solar simulator (EMS-35AAA, Ushio Spax, Inc.). The size of the graphene electrodes was ~ 15 mm × 7 mm, and the active area illuminated with visible light was 3 mm × 3 mm.

As shown in Fig. S4(b), the current density of OPVs with doped graphene electrodes is greater than that of OPVs with pristine graphene electrodes, even though the open-circuit voltage (V_{OC}) has not substantially changed. The photovoltaic performances of the OPVs fabricated with pristine and doped graphene films are summarized in Table SIII. In both SLG and DLG electrodes, the performance characteristics of the OPVs fabricated with doped graphene electrodes, such as their fill factor (*FF*) and power conversion efficiency (PCE), are higher than

those of OPVs fabricated with pristine graphene electrodes. Therefore, the graphene electrodes doped with $Mes_2B^+[(C_6F_5)_4B]^-$ positively affect the OPV performance.

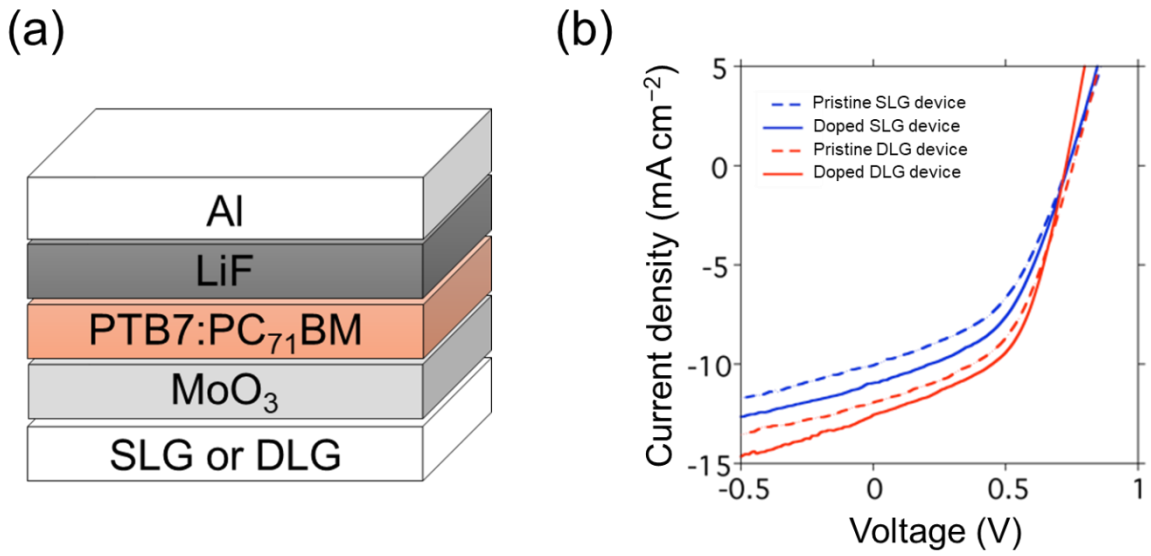

Fig. S4 a Schematic of the OPV device structure. An SLG or DLG electrode is used as the anode material. **b** Current density (J_{SC})–voltage characteristics of OPVs fabricated with pristine (dotted curves) and doped (solid curves) graphene films under simulated sunlight (AM 1.5G).

Table S5. Photovoltaic performance of OPVs fabricated with pristine and doped graphene film electrodes.

Anode	J_{SC} (mA cm^{-2})	V_{OC} (V)	*FF*	PCE (%)
Pristine SLG	10.1	0.74	0.45	3.35
Doped SLG	11.0	0.74	0.47	3.82
Pristine DLG	12.0	0.75	0.48	4.34
Doped DLG	12.6	0.73	0.52	4.73

S8. Calibration of XPS spectra

XPS of the Au $4f_{7/2}$ peak at 84.0 eV is a useful binding energy reference.[6] In particular, the XPS spectrum of the Au 4f region is well separated by spin–orbit interactions, resulting in the XPS Au $4f_{7/2}$ peak at 84.0 eV and the XPS Au $4f_{5/2}$ peak at 87.7 eV.[6] Figure S5 shows the calibrated XPS peaks of pristine and doped graphene samples with gold electrodes. As shown in Fig. S5, the XPS Au $4f_{7/2}$ and Au $4f_{5/2}$ peaks are clearly observed in both pristine and doped graphene samples. Therefore, we used these XPS Au 4f peaks to calibrate the XPS F 1s, B 1s, and C 1s spectra of pristine and doped graphene samples.

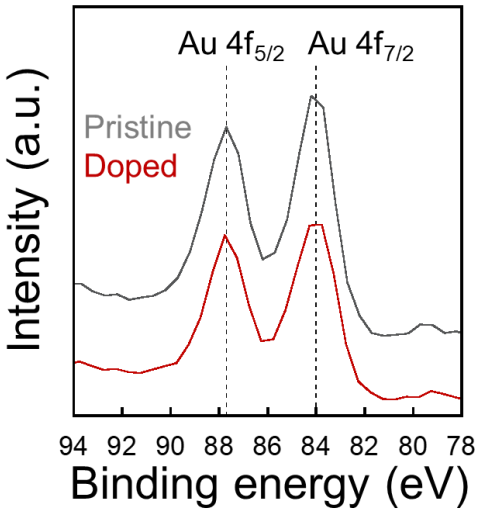

Fig. S5 Calibrated XPS Au 4f peaks for both pristine (gray) and doped (red, Sample #6) graphene samples. The peak positions of XPS Au $4f_{5/2}$ (87.7 eV, left dotted line) and XPS Au $4f_{7/2}$ (84.0 eV, right dotted line) are also indicated.

References

1. Lee, S. *et al*. Wafer Scale Homogeneous Bilayer Graphene Films by Chemical Vapor Deposition. *Nano Lett*. **20**, 4702−4707 (2010).

2. Hao, Y. *et al*. Probing Layer Number and Stacking Order of Few-layer Graphene by Raman Spectroscopy. *Small* **6**, 195−200 (2010).
3. Graf, D. *et al*. Spatially Resolved Raman Spectroscopy of Single- and Few-layer Graphene. *Nano Lett*. **7**, 238−242 (2007).
4. Ago, H. *et al*. Epitaxial Growth and Electronic Properties of Large Hexagonal Graphene Domains on Cu(111) Thin Film. *Appl*. *Phys*. *Express* **6**, 075101 (2013).
5. Takesaki, Y. *et al*. Highly Uniform Bilayer Graphene on Epitaxial Cu−Ni(111) Alloy. *Chem*. *Mater*. **28**, 4583−4592 (2016).
6. Ralf, N. *et al*. Core Level Binding Energies for the Elements Hf to Bi (*Z* = 72-83). *J*. *Phys*. *C*: *Solid State Phys*. **13**, L1091−6 (1980).